High Temperature Ferromagnetism in GaAs-Based Heterostructures with Mn δ Doping

A. M. Nazmul,[1,2] T. Amemiya,[1] Y. Shuto,[1] S. Sugahara,[1] and M. Tanaka[1,2]

[1]*Department of Electronic Engineering, The University of Tokyo, 7-3-1 Hongo, Bunkyo-ku, Tokyo 113-8656, Japan*
[2]*PRESTO/SORST, Japan Science & Technology Agency, 4-1-8 Honcho, Kawaguchi, Saitama 332-0012, Japan*
(Received 25 October 2004; published 28 June 2005)

We show that suitably designed magnetic semiconductor heterostructures consisting of Mn delta (δ)-doped GaAs and p-type AlGaAs layers, in which the locally high concentration of magnetic moments of Mn atoms are controllably overlapped with the two-dimensional hole gas wave function, realized remarkably high ferromagnetic transition temperatures (T_C). A significant reduction of compensative Mn interstitials by varying the growth sequence of the structures followed by low-temperature annealing led to high T_C up to 250 K. The heterostructure with high T_C exhibited peculiar anomalous Hall effect behavior, whose sign depends on temperature.

DOI: 10.1103/PhysRevLett.95.017201 PACS numbers: 75.50.Pp, 71.55.Eq, 72.20.My, 72.25.Dc

The introduction of band gap engineering and wave function engineering into the study of collective magnetic phenomena in semiconductors is opening ways to manipulate the magnetic properties by changing the carrier characteristics such as the wave function, concentration, and carrier spin. For example, ferromagnetic order in the quasi two-dimensional carrier systems of II-VI and III-V based magnetic semiconductor heterostructures can be induced or erased by changing the overlap of the two-dimensional hole gas (2DHG) wave function with the magnetic impurities [1,2]. The magnetization and the ferromagnetic transition temperature (T_C) in these systems can be controlled by changing the carrier concentration with a gate-electric field or by changing the carrier spins by circularly polarized light irradiation [3–5]. Despite such fundamental studies, the material design with T_C near or above room temperature remained one of the most important challenges towards the realization of the semiconductor spintronics.

Theoretical calculations within the mean-field formalism predicted that the T_C can be raised with increasing both the magnetic dopant concentration and the carrier concentration in semiconductors [6,7]. Experimental investigations were carried out to maximize the concentration of Mn substitutionally incorporated in the cation site of GaAs to act as acceptors rather than as compensating interstitial defects. It was reported that long-time annealing of (GaMn)As at low-temperature (LT) ($\leq 200\,^{\circ}$C) can reduce the interstitial defect density, leading to significant improvement in its T_C as high as 159 K [8]. It was also pointed out that the interstitial defect density can be controlled by changing its formation energy with changing the Fermi energy during growth [9]. In this Letter, we show that suitably designed p-type selectively doped III-V heterostructures (p-SDHS) with Mn delta (δ) doping in the 2DHG channel have ferromagnetic order with remarkably high T_C. Here, the δ doping of Mn atoms in semiconductors allows locally high concentration of magnetic moments exceeding the solubility limit in the bulk semiconductor host [10,11]. We found that the growth sequence of the p-SDHS with Mn δ doping and LT annealing for suppressing interstitial defect formation are very important to realize high T_C. We also observed a clear sign change in the anomalous Hall effect (AHE) of the high T_C heterostructure.

We have grown two types of p-SDHS samples with Mn δ doping (sample A and sample B) by molecular beam epitaxy (MBE) on semiinsulating (SI) GaAs(001) substrates. In sample A, a GaAs layer with Mn δ-doped content $\theta_{Mn} = 0.5$ monolayer (ML) ($\theta_{Mn} = 1$ ML corresponds to a sheet Mn concentration of 6.3×10^{14} cm^{-2} [11]) was grown at a substrate temperature T_s of 300 °C on a p-type Be-doped $Al_{0.5}Ga_{0.5}As$ layer (Be concentration $= 1.8 \times 10^{18}$ cm^{-3}, $T_s = 600\,^{\circ}$C), as shown in Fig. 1(a). Here, holes are supplied from the underlying p-AlGaAs layer to the overgrown Mn δ-doped GaAs channel, resembling an inverted high electron-mobility transistor (I-HEMT). Details of the growth procedures are described elsewhere [11]. The thickness d_s of the undoped-GaAs separation layer, which was a measure to control the interaction between the Mn δ-doped GaAs layer and the 2DHG formed at the GaAs/p-AlGaAs interface, was set to 2 nm to enhance

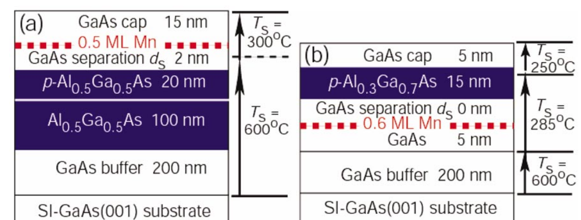

FIG. 1 (color). p-type selectively doped heterostructures (p-SDHS) grown by MBE on SI GaAs(001) substrates: (a) Mn δ-doped ($\theta_{Mn} = 0.5$ ML) GaAs/Be-doped p-AlGaAs heterostructure (I-HEMT type) (sample A). (b) Be-doped p-AlGaAs/Mn δ-doped ($\theta_{Mn} = 0.6$ ML) GaAs heterostructure (N-HEMT type) (sample B).

 © 2005 The American Physical Society

the overlap of the 2DHG wave function and the Mn δ-doped layer [2]. Postgrowth annealing was carried out at 300 °C for 15 min in a N_2 atmosphere, which was optimum to maximize T_C in our previous report [2]. On the other hand, in sample B, a Mn δ-doped ($\theta_{Mn} = 0.6$ ML) GaAs layer was grown at $T_s = 285$ °C below a p-type Be-doped $Al_{0.3}Ga_{0.7}As$ layer (Be concentration $= 3.0 \times 10^{19}$ cm^{-3}), as shown in Fig. 1(b). Here, holes are supplied from the overgrown p-AlGaAs layer to the Mn δ-doped GaAs layer ($d_s = 0$ nm), resembling a normal (N)-HEMT. Postgrowth LT annealing was carried out at 200 °C for 112 h in a N_2 atmosphere.

The structural properties of the Mn δ-doped heterostructures were characterized by high-resolution transmission electron microscopy (HRTEM). Figure 2(a) shows a cross-sectional HRTEM lattice image of a Mn δ-doped GaAs with $\theta_{Mn} = 1$ ML prepared under the same conditions of sample A, in which one can see no dislocation, and a slightly dark area with a width of $\sim$2 ML is most likely due to strain induced contrast at the Mn δ-doped sheet. Also, Figs. 2(b) and 2(c) show cross-sectional HRTEM lattice images of the structure of sample B, indicating that the $Al_{0.3}Ga_{0.7}As$/GaAs interface [we see weak contrast in Fig. 2(b)] is atomically abrupt, and one can see no clusters or dislocations in the whole structure. These studies suggest that pseudomorphic growth of Mn δ-doped sheets occurred maintaining the zinc-blende (ZB) type crystal structure, which is consistent with the reflection high energy electron diffraction patterns observed during the MBE growth of the samples.

The anomalous Hall effect [12] has been used to study the magnetic properties of the present quasi-two-dimensional p-SDHS systems for which bulk magnetization measurements are difficult. Hall measurements were carried out on patterned Hall bars with a channel width and a length of 50 and 200 μm, respectively. Au wire leads were soldered to the sample with In for Ohmic contacts. The postgrowth LT annealing and annealing for Ohmic contacts were done at 200 °C or below, thus excluding the possibility of ferromagnetic MnAs second phase formation. Figs. 3(a)–3(e) show the Hall resistance R_H as a function of magnetic field of sample A. Here, in this system, $R_H = R_{O\text{-sheet}}B + R_{S\text{-sheet}}M$, where $R_{O\text{-sheet}}$ and $R_{S\text{-sheet}}(= cR_{sheet})$ are the ordinary and anomalous Hall coefficients, B is the applied magnetic field, M is the magnetization of the sample, c is a constant, and R_{sheet} is the sheet resistance. The second term is dominant in magnetic materials, thus $R_H \approx R_{S\text{-sheet}}M = cR_{sheet}M$. Clear ferromagnetic hysteresis at 130, 180, 185, and 190 K changed to a linear character at 205 K in Figs. 3(a)–3(e), suggesting a phase transition from ferromagnetic to paramagnetic above 190 K. The positive linear component superimposed on the hysteresis could be due to a slowly saturated magnetization component as is also seen in GaMnAs, which might be attributed to the magnetic polarons as discussed in Ref. [13].

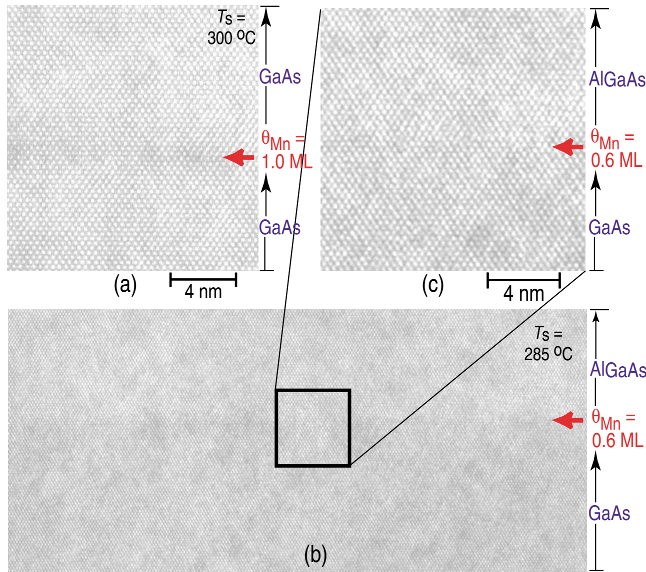

FIG. 2 (color). (a) Cross-sectional HRTEM lattice image of a 1.0 ML Mn δ-doped sheet in GaAs grown under the same conditions of sample A ($T_s = 300$ °C). The slightly dark area indicated by arrows corresponds to the Mn δ-doped sheet localized within a width of 2–3 ML. (b),(c) Cross-sectional HRTEM lattice image of the $Al_{0.3}Ga_{0.7}As$/GaAs heterostructure with $\theta_{Mn} = 0.6$ ML (sample B: $T_s = 285$ °C). (c) is an enlarged image at the Mn δ-doped layer. There is no dislocation, no visible second phase or MnAs clusters, and the structure maintains the zinc-blende type crystal structure.

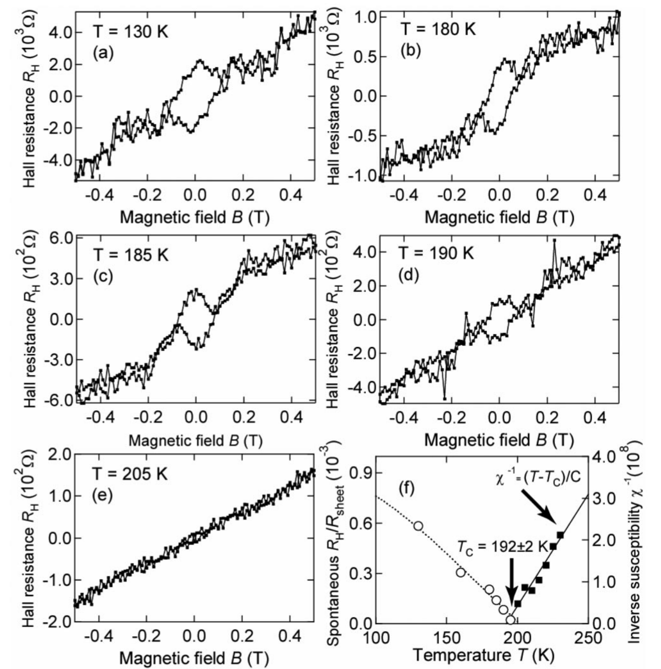

FIG. 3. (a)–(e) Hall resistance R_H loops of the heterostructure of Fig. 1(a) at (a) 130, (b) 180, (c) 185, (d) 190, and (e) 205 K. (f) Temperature (T) dependent data of $R_H(B = 0\ T)/R_{sheet}(\propto M)$ at $T < T_C$, and also of $BR_{sheet}/R_H(\propto \chi^{-1})$ at $T > T_C$. The linear plot is $\chi^{-1}[= (T - T_C)/C]$, where $T_C = 192$ K.

The T_C of the heterostructure was estimated from the temperature (T) dependence of spontaneous magnetization $M(B=0)$ derived from the data of $R_H(B=0)/R_{sheet}$ for $T < T_C$, as shown by the open circles in Fig. 3(f). Also, the temperature dependence of inverse magnetic susceptibility χ^{-1} was derived from the data of BR_{sheet}/R_H for $T > T_C$, where the sample is paramagnetic, thus $M = \chi B/\mu_0$. Assuming that R_O is T independent in the Curie-Weiss equation [2], we plotted χ^{-1} as a function of T, as shown by the solid squares in Fig. 3(f). By extrapolating the fit of $\chi^{-1} = \frac{T-T_C}{C}$ to cross the T axis in Fig. 3(f), the T_C value is estimated to be 192 ± 2 K, which is in good agreement with the spontaneous $R_H/R_{sheet} - T$ data for $T < 200$ K [Figs. 3(a)–3(e) and open circles in Fig. 3(f)]. In this estimation, we set the Mn content $x = 0.25$ for $\theta_{Mn} = 0.5$ ML (since we defined the local Mn content as $\theta_{Mn}/2$ ML, where 2 ML is the width of Mn distribution along the growth direction estimated by TEM [2,11]). The Curie-Weiss plot fitted the experimental data assuming the skew scattering as the dominant scattering mechanism ($R_{S\text{-}sheet} = cR_{sheet}$ [2]) better than assuming the side-jump scattering ($R_{S\text{-}sheet} = c{R_{sheet}}^2$).

We observed an increase of T_C from our previous report of $T_C = 172$ K in a similar I-HEMT type heterostructure (0.3 ML Mn δ-doped GaAs/Be-doped p-$Al_{0.3}Ga_{0.7}As$ [2]). The differences in structural parameters are the following: $\theta_{Mn} = 0.3$ ML, Al content x_{Al} in the p-AlGaAs is 0.3, and $d_s = 0$ nm in the previous heterostructure, but, in sample A, $\theta_{Mn} = 0.5$ ML, $x_{Al} = 0.5$, and $d_s = 2$ nm. Three important differences are that sample A has a higher Mn concentration (θ_{Mn}) in δ doping, a higher GaAs/p-AlGaAs valence-band offset $\Delta E_v = 300$ meV compared with 180 meV in the previous heterostructure due to the difference in x_{Al}, and an appropriate separation of $d_s = 2$ nm. The sheet hole concentration p was estimated to be $7.8 \pm 0.5 \times 10^{12}$ cm^{-2} at room temperature from the ordinary Hall coefficient ($R_{O\text{-}sheet} = 80\ \Omega/\mathrm{T}$). This value is higher than the previous value $p = 2.2 \times 10^{12}$ cm^{-2} [2]. The combined effects of increased Mn concentration, increased hole concentration, and enhanced 2DHG-Mn overlap led to the higher T_C in the present I-HEMT structure of sample A.

Next, we examined sample B of Fig. 1(b), which is a N-HEMT type heterostructure with Mn δ doping. Figure 4(a) shows the temperature dependence of the sheet resistance R_{sheet} of sample B. The hump at around 250 K is attributed to the critical scattering nearby T_C [14], as was seen in (GaMn)As [13]. Figs. 4(b)–4(d) measured at 235, 240, and 250 K show clear ferromagnetic hysteresis in the Hall resistance ($R_H - B$) loops. This ferromagnetic hysteresis behavior changed to paramagnetic behavior at 260 K [Fig. 4(e)] indicating $T_C \cong 250$–255 K, which is in agreement with the hump in Fig. 4(a) at around 250 K.

We ascribe the remarkably high T_C of sample B to both increased Mn concentration ($\theta_{Mn} = 0.6$ ML) and reduced compensative Mn interstitials (Mn_I). It is pointed out that

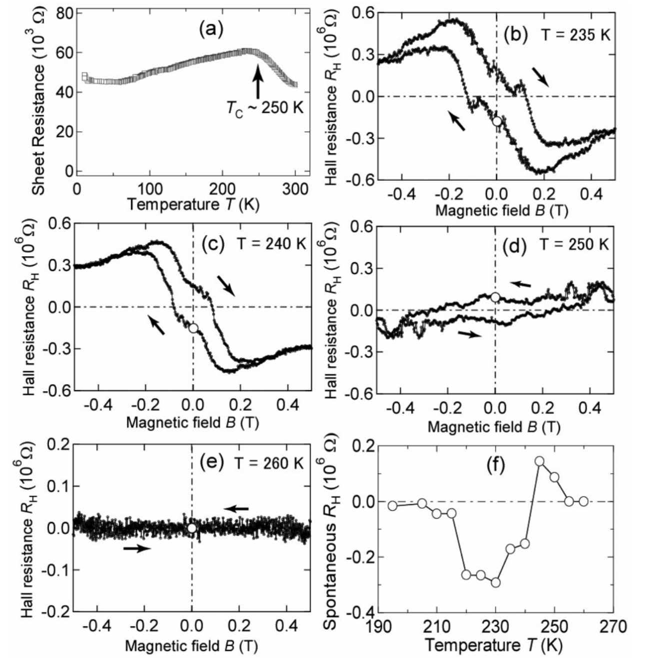

FIG. 4. (a) Temperature dependence of the sheet resistance R_{sheet} of sample B whose structure is shown in Fig. 1(b). (b)–(e) Hall resistance R_H loops of sample B measured at (b) 235, (c) 240, (d) 250, and (e) 260 K. (f) Temperature dependence of the spontaneous Hall resistance R_H at $B = 0$ T [also shown by open circles in (b)–(e)].

Mn atoms can occupy tetrahedral interstitial sites (Mn_I) in the ZB structure and act as double donors [15,16]. The compensation of Mn acceptors at the Mn substitutional sites (Mn_{Ga}) by the Mn_I donors decreases the hole concentration p and T_C. The effect of the Fermi energy can have the significant contribution to the suppression of interstitial defect formation in the N-HEMT type of sample B, compared with that in the I-HEMT type of sample A. It is reported that the formation energies and thus the concentrations of charged (positive or negative) defects such as Mn_I donors or Mn_{Ga} acceptors are to a large extent controlled by the Fermi energy during growth [9]. In the I-HEMT structure in which the Mn δ-doped GaAs was grown after the growth of p-AlGaAs, Mn_{Ga} formation becomes unfavorable during the Mn δ doping growth because it further increases the hole concentration, and a high concentration of compensating Mn_I defects are formed instead to balance the charge. This scenario turns opposite in the N-HEMT structure, making Mn_{Ga} formation energetically favorable because the p-AlGaAs layer supplying holes was grown after the growth of the Mn δ-doped layer. Recently, Edmonds *et al.* [8] showed that the outdiffusion of the Mn_I in (GaMn)As films strongly depends on the thickness of the film; with increasing film thickness, longer LT annealing at $\leq 200\,^\circ$C is more effective to remove Mn_I and to increase T_C. In fact, the sheet hole concentration of sample B at room temperature was $p = 7.2 \pm 0.5 \times 10^{13}$ cm^{-2} [17], much higher than that of

sample A, leading to the metallic behavior of Fig. 4(a). It is also pointed out that the arsenic antisite (As_{Ga}) defects do not play a significant role in LT annealing, since As_{Ga} defects remain stable up to 450 °C [18]. Therefore, coupled with the Mn_I diffusion during the long LT annealing treatment and the increase of Mn concentration, the above scenarios can explain the large difference of T_C in the I-HEMT type ($T_C = 192$ K) and the N-HEMT type ($T_C \sim 250$ K) heterostructures.

We observed a clear sign change of AHE in sample B, as shown in Figs. 4(b)–4(d). Figure 4(f) shows the temperature dependence of the spontaneous Hall resistance $R_H(B = 0$ T). Here, the spontaneous R_H is defined as the Hall resistance at $B = 0$ T due to the spontaneous magnetization, after a positive magnetic field ($B = 0.5$ T) is applied and B is then reduced to 0 T, as shown by the open circles in Figs. 4(b)–4(e). As seen in Fig. 4(f), the spontaneous R_H varies nonmonotonously with T, and its sign is negative at $T \leq 240$ K and positive at $T \geq 245$ K. The features of the sign change and nonmonotonous behavior in the $R_H - T$ data could be due to the contribution of the Berry-phase effect to the AHE. Very recently, it has been suggested that the Berry-phase effect in the crystal momentum space can also give rise to AHE [19–22] and can explain the AHE in (III,Mn)V magnetic semiconductors [19] and metallic $SrRuO_3$ [20]. Here, the Berry-phase does not involve scattering, but depends on the Bloch states in the Fermi surface, and the Hall resistivity ρ_H can be described as $\rho_H = -\rho^2\sigma_H(M)$, where the Hall conductivity σ_H does not depend on longitudinal resistivity ρ and its dependence on M should be calculated from the band structure. The features of the sign change and the nonmonotonous behavior in the $R_H - T$ data of sample B in Fig. 4(f) are similar to those observed in metallic $SrRuO_3$ ferromagnets, where first-principles calculations of the Berry-phase contribution to the AHE showed excellent agreement with the experimental data [20]. It is noteworthy that in other Mn δ-doped p-SDHSs (not shown here), we observed positive and monotonous behavior in the $R_H - T$ data in the case of semiconductive samples as was the case of sample A, and the sign change and nonmonotonous behavior become significant in metallic samples as was the case of sample B. The difference between semiconductive samples and the metallic samples is in the nature of the quasiparticle's behavior; the metallic sample B with higher hole concentration and higher Mn coverage probably has significant valence-band mixing with increased Fermi-surface curvature [19], leading to an observable Berry-phase contribution to the AHE.

In the $R_H - B$ hysteresis loops of Figs. 4(b)–4(d), step-like features appeared at around ± 0.1 T. One might attribute such steps to the influence of domain pinning in the MnAs clusters as the possible second phase. However, the possibility of MnAs cluster formation can be excluded by our study of HRTEM lattice images [for example, see Figs. 2(b) and 2(c)]. Instead, the presence of an inclined magnetic easy axis due to magnetocrystalline anisotropy of the system, as usually is seen in GaMnAs with in-plane magnetization easy axis, could explain the origin of the step that appears during the magnetization reversal process under the external magnetic field perpendicular to the film. Another possibility is the influence of domain-wall pinning at the patterned Hall bar edges during the motion of domain walls in magnetization reversal.

In conclusion, the large enhancement of T_C using both I-HEMT and N-HEMT structures presented here can provide opportunities for fundamental studies in the magnetic quasi-two-dimensional systems, and can also lead to functional device applications complying with the present semiconductor technology.

[1] A. Haury *et al.*, Phys. Rev. Lett. **79**, 511 (1997).

[2] Ahsan M. Nazmul, S. Sugahara, and M. Tanaka, Phys. Rev. B **67**, 241308 (2003).

[3] H. Ohno *et al.*, Nature (London) **408**, 944 (2000).

[4] S. Koshihara *et al.*, Phys. Rev. Lett. **78**, 4617 (1997); A. Oiwa *et al.*, Phys. Rev. Lett. **88**, 137202 (2002).

[5] Ahsan M. Nazmul, S. Kobayashi, Sugahara, and M. Tanaka, Jpn. J. Appl. Phys. **43**, L233 (2004).

[6] T. Dietl *et al.*, Science **287**, 1019 (2000).

[7] Van an Dinh, K. Sato, and H. Katayama-Yoshida, Jpn. J. Appl. Phys. **42**, L888 (2003).

[8] K. W. Edmonds *et al.*, Phys. Rev. Lett. **92**, 037201 (2004).

[9] K. M. Yu *et al.*, Phys. Rev. B **65**, 201303 (2002); W. Walukiewicz, Appl. Phys. Lett. **54**, 2094 (1989).

[10] R. K. Kawakami *et al.*, Appl. Phys. Lett. **77**, 2379 (2000).

[11] Ahsan M. Nazmul, S. Sugahara, and M. Tanaka, Appl. Phys. Lett. **80**, 3120 (2002); J. Cryst. Growth **251**, 303 (2003).

[12] L. Berger and G. Bergmann, *The Hall Effect and Its Applications*, edited by C. L. Chien and C. R. Westgate (Plenum, New York, 1980), p. 55.

[13] A. Oiwa *et al.*, Solid State Commun. **103**, 209 (1997).

[14] M. E. Fisher *et al.*, Phys. Rev. Lett. **20**, 665 (1968).

[15] F. Máca and J. Mašek, Phys. Rev. B **65**, 235209 (2002).

[16] S. C. Erwin and A. G. Patukhov, Phys. Rev. Lett. **89**, 227201 (2002).

[17] This value was estimated by assuming the same mobility $\mu = 1.9$ cm^2/V s both in sample A and sample B, since the high T_C of sample B made it difficult to rule out the anomalous Hall effect contribution in Curie-Weiss fitting to estimate p and μ. Our other Mn δ-doped p-SDHS samples (not shown here) of both the I-HEMT and the N-HEMT type with relatively low T_C are found to have similar μ values (2–5 cm^2/V s), and thus supporting our assumption.

[18] D. E. Bliss *et al.*, J. Appl. Phys. **71**, 1699 (1992).

[19] T. Jungwirth, Q. Niu, and A. H. MacDonald, Phys. Rev. Lett. **88**, 207208 (2002).

[20] Z. Fang *et al.*, Science **302**, 92 (2003).

[21] Y. Yao *et al.*, Phys. Rev. Lett. **92**, 037204 (2004).

[22] Byounghak Lee, T. Jungwirth, and A. H. MacDonald, Semicond. Sci. Technol. **17**, 393 (2002).